Topological Mechanics of Origami and Kirigami

Bryan Gin-ge Chen,[1,*] Bin Liu,[2,†] Arthur A. Evans,[3,‡] Jayson Paulose,[1]
Itai Cohen,[2] Vincenzo Vitelli,[1] and C. D. Santangelo[3]

[1]*Instituut-Lorentz, Universiteit Leiden, 2300 RA Leiden, The Netherlands*
[2]*Department of Physics, Cornell University, NewYork 14853, USA*
[3]*Department of Physics, University of Massachusetts, Amherst, Massachusetts 01002, USA*
(Received 5 August 2015; published 30 March 2016)

Origami and kirigami have emerged as potential tools for the design of mechanical metamaterials whose properties such as curvature, Poisson ratio, and existence of metastable states can be tuned using purely geometric criteria. A major obstacle to exploiting this property is the scarcity of tools to identify and program the flexibility of fold patterns. We exploit a recent connection between spring networks and quantum topological states to design origami with localized folding motions at boundaries and study them both experimentally and theoretically. These folding motions exist due to an underlying topological invariant rather than a local imbalance between constraints and degrees of freedom. We give a simple example of a quasi-1D folding pattern that realizes such topological states. We also demonstrate how to generalize these topological design principles to two dimensions. A striking consequence is that a domain wall between two topologically distinct, mechanically rigid structures is deformable even when constraints locally match the degrees of freedom.

Recent interest in origami mechanisms has been spurred by advances in fabrication and manufacturing [1–3], as well as a realization that folded structures can form the basis of mechanical metamaterials [4–8]. The ability to identify kinematic mechanisms—allowable folding motions of a crease pattern—is critical to the use of origami to design new deployable structures and mechanical metamaterials. For example, the mechanism in the celebrated Miura ori that allows it to furl and unfurl in a single motion [9,10] is also the primary determinant of the fold pattern's negative Poisson ratio [4,5]. Identifying these mechanisms becomes more challenging when the number of apparent constraints matches the number of degrees of freedom (DOF).

When there is an exact balance between DOF and constraints in a periodic structure, the structure is marginally rigid [11,12]. In such a case, new mechanical properties such as nonlinear response to small perturbations emerge [13–16]. A recent realization is that the flexibility of such solids may be influenced by nontrivial topology in the phonon band structure [17,18]. Here, we show how to extend these topological ideas to origami and kirigami. We show that periodically folded sheets may exhibit distinct mechanical "phases" characterized by a topological invariant called the *topological polarization*, recently introduced by Kane and Lubensky [17] using a mapping of mechanically marginal structures to topological insulators [19]. The importance of this invariant has emerged in the study of the soft modes of spring networks [18], and the nonlinear mechanics of linkages [20] and buckling [21]. As in these examples, the phases in our origami and kirigami structures exhibit localized vibrational modes on certain boundaries,

and transitions from between topological phases are characterized by the appearance of bulk modes that cost zero energy. These are the hallmarks of topologically protected behavior in classical mechanical systems [22–29]. Topology provides a new knob to tune how materials and, as we show here, origami and kirigami structures, respond to external perturbations.

We denote by *origami*, mechanical structures consisting of rigid flat polygonal plates joined by hinges. We will first discuss origami with no missing plates or "holes," and then generalize to *kirigami*, defined to be origami where such holes are allowed. We will consider the mechanics of origami in the geometrical limit—folds will cost zero energy and faces do not stretch or bend.

To demonstrate the power of our approach, we introduce an example of a 1D strip of origami analogous to the Su-Schrieffer-Heeger polyacetylene model [17,30]. It admits localized modes and stresses determined and protected by topology, which we realize and characterize in experiments. Additionally, we show how to generalize this to 2D periodic origami sheets, where we have observed a striking property that causes origami without holes to have zero topological polarization. We give examples of hinged structures with holes (kirigami) that do admit distinct polarizations and thus can be used as building blocks for metasheets with programmable local flexibility.

Quasi-1D origami strip.—We start with a simple quasi-1D origami structure. Consider an origami strip of zig-zagging rigid quadrilateral plates, depicted in Fig. 1, consisting of a periodically repeating unit cell of two fourfold vertices. Each vertex in a cell (labeled by
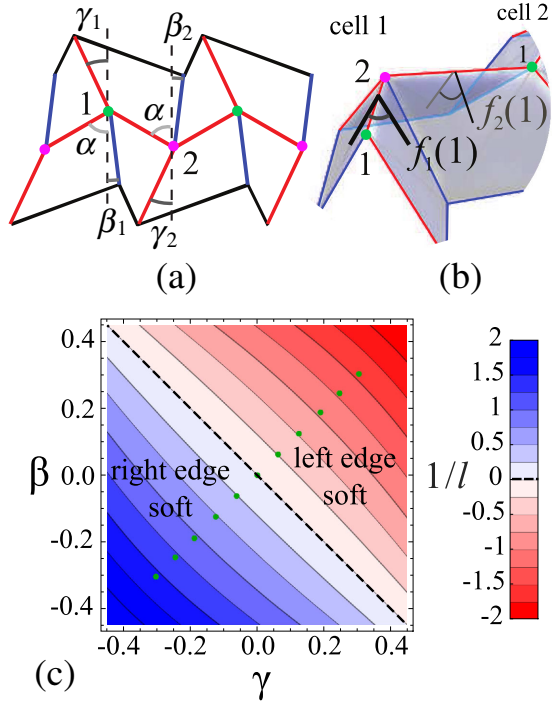
FIG. 1. A quasi-1D origami strip. (a) A unit cell of the fold pattern corresponding to the origami mechanism with planar angles labeled. Red (blue) creases are mountain (valley) folds, respectively. (b) A 3D depiction of a part of the strip with folding angles $f_i(n)$ labeled. (c) The phase diagram where $\alpha = \pi/3$, $\beta \equiv \beta_1 = \beta_2$, and $\gamma \equiv \gamma_1 = \gamma_2$. The colors indicate the phase (blue for right-localized, red for left-localized); the contours and intensity of color follow the inverse decay length $1/l$ (see legend). Configurations where folds at a vertex become collinear lie on $\gamma = \beta$, and the green points along that line were constructed in experiment [along this line, (γ, β) and $(-\gamma, -\beta)$ are related by a rotation in three dimensions].

$n = 1, 2$) has four creases [Fig. 1(a)], and one DOF [31] that we track with the dihedral angles of the bolded crease, $f_n(j)$, where j indexes the unit cell [Fig. 1(b)]. Each adjacent pair of dihedral angles is coupled by the kinematics of the intervening vertex. As each vertex contributes a DOF and a constraint, this origami structure has marginal rigidity.

We analyze the mechanical response of the origami strip by determining its configurations analytically as functions of the fold pattern angles $\beta_1, \beta_2, \gamma_1$, and γ_2 [defined in Fig. 1(a)]. We define a generalized displacement $u(j) = \cos f_2(j) + 1$. The function $u(j)$ encodes the dihedral angle f_2 of the rightmost fold of unit cell j, and satisfies

$$u(j+1) = \kappa(\alpha, \beta_1, \beta_2, \gamma_1, \gamma_2)u(j), \qquad (1)$$

where

$$\kappa = \left[\frac{\sin(\alpha - \beta_1)\sin(\alpha - \gamma_1)}{\sin(\alpha + \beta_1)\sin(\alpha + \gamma_1)}\right]\left[\frac{\sin(\alpha - \beta_2)\sin(\alpha - \gamma_2)}{\sin(\alpha + \beta_2)\sin(\alpha + \gamma_2)}\right].$$
$$(2)$$

The derivation is an application of the spherical law of cosines and is given in the Supplemental Material [32]. The fact that $u(j)$ determines $u(j + 1)$ implies that the strip has 1 degree of freedom, globally. Equation (1) is solved by an exponential $u(j) = u(0)\exp[j\ln(\kappa)]$ with deformation localized to one side or the other, following the sign of the inverse decay length $l^{-1} = \ln \kappa$.

The mechanical "phase diagram" in Fig. 1(c) shows the values of l^{-1} for patterns with $\gamma_1 = \gamma_2 \equiv \gamma$, $\beta_1 = \beta_2 \equiv \beta$. There are two phases distinguished by the sign of $\ln \kappa$, which is determined here by the sign of $\gamma + \beta$, a quantity not obviously related to any symmetry breaking. When $\gamma + \beta > (<)0$, $\kappa < (>)1$, and by Eq. (1), the mechanical response is localized to the left (right) of the origami strip. A special role is played by fold patterns with $\kappa = 1$, where the decay length diverges and $u(j)$ neither grows nor shrinks (denoted by the dashed line). This is precisely the condition for which a global kinematic mechanism exists and the fold pattern is *deployable* [33]. As an example, when $\gamma = \beta = 0$, the strip realizes a row of the Miura ori fold pattern, which has a single collapse motion. More generically, however, as long as $\ln \kappa$ never changes sign, the deformation in a strip, $u(j)$, is localized even if the values of $\alpha, \beta_j, \gamma_j$ vary due to disorder or imperfections, i.e., as long as the material remains within the same phase. The existence of phases of robust, boundary-localized zero-energy deformations separated by critical configurations with bulk zero modes suggests that the origami strip has topologically protected properties.

To make the topology explicit, we calculate a topological invariant of the above phases. Unlike in periodic spring networks with marginal rigidity [17,34,35], a linear analysis is inadequate to capture the topology of the origami strip. Coplanar hinges in the flat state are redundant constraints, and this results in extra zero modes at linear order which do not extend to higher order. In the Supplemental Material [32], we derive a rigidity matrix capturing the *second-order* deformations of this structure and show that it has the same pattern of entries as the Hamiltonian of the Su-Schrieffer-Heeger chain of Refs. [17,30]. Therefore, phases of the origami strip are characterized by their topological polarization $\vec{P}_T$ [17,18], defined as a winding number of the determinant of the rigidity matrix [36]. Indeed, the sign of $\ln \kappa$ is precisely correlated with the topological polarization, and thus the fact that different edges are soft or stiff in different phases is a manifestation of the bulk-boundary correspondence [19] in this system. While topological modes in 1D linkages have been found to lead to propagating domain walls [20,37], this is not possible for our 1D strip. In Eq. (2), κ depends only on the fold pattern angles $\alpha, \beta_j, \gamma_j$, not the dihedral angles f_j—this means that the topological polarization of the unit cell cannot change via the zero-energy deformations, which would be necessary for propagation.

To test the consequences of Eq. (1) away from the ideal limit, in a structure where faces can bend and hinges can

twist, a mylar sheet (200 μm thick) is perforated by a laser cutter into the desired crease pattern, rendering it foldable along lines of perforations. We strengthen the facets by sandwiching the mylar sheet between pairs of 1 mm thick, plastic plates made of polylactic acid (PLA) on a 3D printer. To mount the plastic plates onto the mylar sheet, we use a pushed-in clip design: one facet has clips and the corresponding facet has holes. Equivalent holes are cut on the mylar sheet so that the clips can be pushed through to meet the holes on the plate on the other side of the mylar. An example of the assembled origami structure is shown in Fig. 2(a). Here, we fixed the angle $\alpha = \pi/3$ and varied $\gamma \equiv \beta_1 = \gamma_1 = \beta_2 = \gamma_2$ to explore the localization of the deformation within one phase (with $\kappa < 1$) [38]. A video camera captured the deformation of the strip from above as it was symmetrically compressed. The position of each vertex was obtained via image analysis, and fit with a 3D model to reconstruct the complete morphology of the origami strip, as shown in Fig. 2(b). Finally, the folding angles along the interior creases were extracted from the 3D shape and were used to compute the generalized strain u. Figure 2(c) shows the strain as a function of distance along
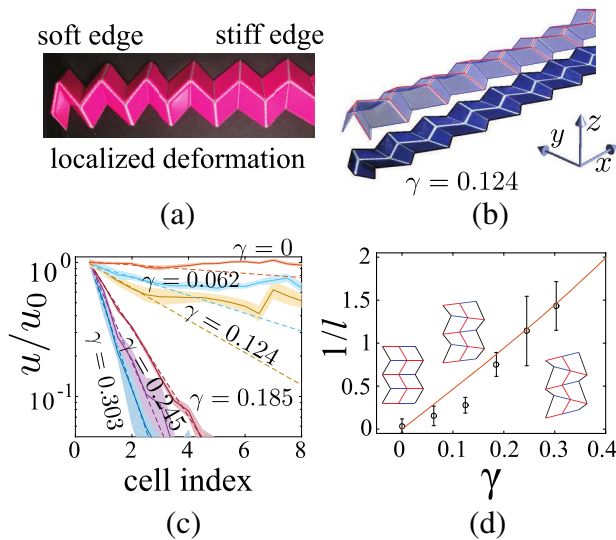

FIG. 2. (a) Localized deformations in an experimental realization of the origami strip ($\alpha = \pi/3$, $\gamma_1 = \gamma_2 = \beta_1 = \beta_2 = 0.062$). (b) 3D reconstruction of the configuration of the strip from a flat image ($\gamma = 0.124$). (c) Normalized generalized strain u/u_0 as a function of distance from the deformable boundary (measured in number of unit cells) from experiments (shaded curves) with fits to an exponential decay (dashed lines). Each curve shows the average of data from 6 to 30 experimental images and has a width equal to the standard error. Folding angles $f_2(1)$ [related to u_0 via $u_0 = 1 + \cos f_2(1)$] at cell 1 varied from 1.06 to 1.45. (d) Inverse decay lengths ($1/l$) versus γ, where data points are averages over the fitting coefficients of all images for each γ and error bars show 95% confidence bounds. The analytical result for $l^{-1} = \ln \kappa$ [Eq. (2)] is plotted as a solid red line. The deviations for small γ arise from a "uniform bending mode" (see text).

the strip for samples with different values of the pattern parameter γ. Observe that there is a "soft" edge (cell index 0), where the deformation is high, and on the other end a "stiff" edge, with low deformation.

As shown by a semilog fit [dashed lines in Fig. 2(c)], the strains decay exponentially at small distances from the soft edge. For small γ, the folding angles level off to a roughly constant value at larger distances, which violates Eq. (1). The constant folding angle background corresponds to the activation of a mode with uniform deformation. This mode is easy to excite as it is the zero energy mode at $\gamma = 0$ and thus remains very low energy for small γ. A deviation from the ideal geometrical limit is possible due to the finite flexibility of the facets and the finite crease thicknesses. Despite the nonideality of the experimental origami strip, the decay lengths extracted from the fit are in good agreement with $1/l = \ln \kappa$ [Fig. 2(d)], confirming the robustness of our topological design principle.

Two-dimensional origami.—Having established that marginally rigid 1D periodic origami can exhibit topological phases, we now ask whether marginality also leads to similar phases in 2D origami. We first characterize the class of *marginally rigid* 2D periodic origami and show that they must have a triangulated crease pattern. To avoid trigonometric complexity inherent to a folding angle representation, we model the kinematics of triangulated origami as a central-force spring network with vertices as joints and hinges as springs. Triangles in such a network automatically enforce the no-bending constraint on the facets. Arbitrary origami can be modeled with spring networks, but nontriangular faces require additional internal springs to remain rigid.

In this framework, each joint has 3 degrees of freedom and each spring adds one constraint, so marginal structures satisfy $E = 3V$ where E is the number of bonds and V is the number of joints. In a triangulated surface without a boundary, each of the F faces is a triangle, so $3F = 2E$. The Euler characteristic χ is defined as $\chi = V - E + F$; thus we obtain $E = 3(V - \chi)$.

Periodic origami structures in two dimensions have the topology of the torus and thus $\chi = 0$, which shows that triangulations are marginally rigid. While achieving marginality in granular packings and glassy networks requires some fine-tuning in pressure or coordination, the analogous origami triangulations arise naturally. Any nontriangular plate in an origami pattern can be triangulated by adding diagonals, and the bending of nontriangular plates in real origami can be modeled as the addition of new creases [4,6].

One might now expect a variety of topological phases upon changing the angles and lengths of a triangulated crease pattern, by analogy with the 1D strip. Surprisingly, our calculations indicate otherwise. As discussed above, an analysis of the rigidity of *flat* origami must go beyond linear order. To bypass this complication, we consider periodic triangulated origami where we break the flat-state

degeneracy by introducing small vertical displacements to the vertices. The linear rigidity and topological properties of such a structure can then be expressed in terms of the (Fourier-transformed) rigidity matrix $\mathbf{R}$ for its associated spring network [17,18]. However, for all triangulated periodic fold patterns we have considered, the function $\det \mathbf{R}(\mathbf{q})$, *a priori* a complex-valued function, is in fact real valued for all $\mathbf{q}$ in the Brillouin zone [39]. Though a proof of this statement for all triangulated origami eludes us, extensive numerical tests on a large number of distinct fold patterns bear out this conjecture. We give details and partial results in the Supplemental Material [32].

A consequence of the "reality" property is that the winding numbers of Arg $\det \mathbf{R}(\mathbf{q})$ along any closed curves in the Brillouin zone must be zero (when defined), and, hence, the topological polarization $\vec{P}_T$ must vanish. Localized boundary modes for such origami still exist, but must be isotropically distributed. Even if the hinges in a unit cell break left-right symmetry, the number of boundary modes per unit cell on each edge of a finite patch is left-right and up-down symmetric. If in fact all triangulated periodic origami structures have this property, the only way to get an imbalance in the number of zero modes at the boundary of origami is by locally adding or removing constraints. This behavior contrasts with that of the 1D strip of origami studied above as well as 3D periodic networks and marginal spring networks confined to 2D.

Topological kirigami.—Thus the question remains: do there even exist 2D periodic hinged structures with a nonzero topological polarization? The answer is yes, but we must go beyond origami to *kirigami*, folded structures with holes. There is a simple way to generate marginal kirigami from triangulated origami. Cutting out an adjacent pair of triangles removes one bond from the associated spring network, eliminating a constraint. Likewise, merging two triangles into a rigid quadrilateral plate adds a constraint. We therefore modify a triangular lattice by cutting and merging twice, resulting in a structure with two quadrilateral plates and two quadrilateral holes per unit cell (top center of Fig. 3). Now $\det \mathbf{R}(\mathbf{q})$ is complex-valued, and by randomly perturbing a flat realization, we find the "green" (left) and "blue" (right) structures depicted in Fig. 3, which have $\vec{P}_T = (1,0)$ and $(0,0)$, respectively (see Supplemental Material [32] for more details). With free boundary conditions, the boundary soft modes in the green kirigami are polarized to the $+x$ edge (analogous to the 1D strip and in contrast to the blue kirigami and all triangulated origami structures we tested).

Finding the green kirigami answers the question above positively, and we leave a determination of the possible phases that can occur in the modified triangular lattice to future work. A full characterization will likely be difficult due to the high dimensionality of the realization space (cf. Ref. [40], which shows the complexity of the phase diagram in a simpler mechanical system). We thus switch
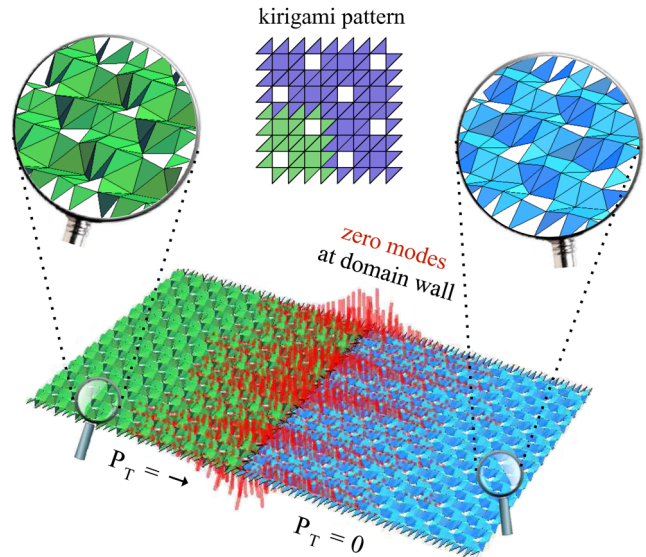

FIG. 3.   Topologically protected zero mode (red) in a kirigami heterostructure [left green with topological polarization $\vec{P}_T = (1,0)$ / right blue with $\vec{P}_T = (0,0)$]. Numerically the mode depicted has energy nearly indistinguishable from the translation modes. This is a close-up of a larger periodic 50×5 system, divided into two 25×5 domains (two copies in the shorter direction are shown). The magnifying glass insets show the fine structure of four unit cells of each type, and between them is a schematic showing how the quadrilateral plates, strips of triangles, and quadrilateral holes are joined by hinges. The schematic shows four unit cells, with the lower left cell highlighted in green.

gears and present an example of localized modes designed into a kirigami "heterostructure" to illustrate the power of our techniques. In Fig. 3, we show a kirigami structure that exhibits zero modes localized at a domain wall (one per unit cell) between the two kirigami structures described above. The zero modes render the heterostructure flexible in the vicinity of the domain wall (the mode depicted leads to out-of-plane wrinkling), while keeping it rigid further away. By contrast, a domain wall between distinct patterns with equal polarization has no such localized modes (see Supplemental Material [32]). In general, domain walls between structures with different polarizations create either soft lines along which the system easily deforms, or "stressed" lines which first bear the loads under applied strains [21]. Similar effects may arise at point defects in otherwise uniform polarized structures [41].

Outlook.—We have demonstrated that origami and kirigami structures are characterized by a topological polarization that classifies the ways that a marginally rigid fold pattern can be floppy close to its boundaries. Our results give strong constraints on the types of boundary modes that can be created in origami and will guide the design of fold patterns that achieve a targeted mechanical response. In the design space of geometric realizations, two

structures with different polarizations must be separated by globally flexible, i.e., deployable, realizations. Thus not only can structures with distinct phases be combined in real space to form domain walls with useful functionality, but also they can be used to find deployable patterns in design space. These realization spaces are high dimensional in general, so the problem of determining simple rules to create a given polarization remains open.

---

[*]Current Address: Department of Physics, University of Massachusetts, Amherst, MA 01002, USA.

[†]Current Address: School of Natural Sciences, University of California, Merced, CA 95343, USA.

[‡]Current Address: Department of Mathematics, University of Wisconsin, Madison, WI 53706, USA.

[1] J. Ryu, M. D'Amato, X. Cui, K. N. Long, H. J. Qi, and M. L. Dunn, Appl. Phys. Lett. **100**, 161908 (2012).

[2] M. T. Tolley, S. M. Felton, S. Miyashita, D. Aukes, D. Rus, and R. J. Wood, Smart Mater. Struct. **23**, 094006 (2014).

[3] Y. Liu, M. Miskiewicz, M. J. Escuti, J. Genzer, and M. D. Dickey, J. Appl. Phys. **115**, 204911 (2014).

[4] Z. Y. Wei, Z. V. Guo, L. Dudte, H. Y. Liang, and L. Mahadevan, Phys. Rev. Lett. **110**, 215501 (2013).

[5] M. Schenk and S. D. Guest, Proc. Natl. Acad. Sci. U.S.A. **110**, 3276 (2013).

[6] J. L. Silverberg, A. A. Evans, L. McLeod, R. C. Hayward, T. Hull, C. D. Santangelo, and I. Cohen, Science **345**, 647 (2014).

[7] C. Lv, D. Krishnaraju, G. Konjevod, H. Yu, and H. Jiang, Sci. Rep. **4**, 5979 (2014).

[8] S. Waitukaitis, R. Menaut, B. G. Chen, and M. van Hecke, Phys. Rev. Lett. **114**, 055503 (2015).

[9] K. Miura, Proc. 31st Congr. Int. Astronaut. Federation **IAF-8 0-A 31**, 1 (1980).

[10] A. A. Evans, J. L. Silverberg, and C. D. Santangelo, Phys. Rev. E **92**, 013205 (2015).

[11] C. S. O'Hern, L. E. Silbert, A. J. Liu, and S. R. Nagel, Phys. Rev. E **68**, 011306 (2003).

[12] S. Alexander, Phys. Rep. **296**, 65 (1998).

[13] M. Wyart, S. Nagel, and T. Witten, Europhys. Lett. **72**, 486 (2005).

[14] M. Wyart, H. Liang, A. Kabla, and L. Mahadevan, Phys. Rev. Lett. **101**, 215501 (2008).

[15] L. R. Gómez, A. M. Turner, M. van Hecke, and V. Vitelli, Phys. Rev. Lett. **108**, 058001 (2012).

[16] S. Ulrich, N. Upadhyaya, B. van Opheusden, and V. Vitelli, Proc. Natl. Acad. Sci. U.S.A. **110**, 20929 (2013).

[17] C. Kane and T. Lubensky, Nat. Phys. **10**, 39 (2014).

[18] T. Lubensky, C. Kane, X. Mao, A. Souslov, and K. Sun, Rep. Prog. Phys. **78**, 073901 (2015).

[19] M. Z. Hasan and C. L. Kane, Rev. Mod. Phys. **82**, 3045 (2010).

[20] B. G. Chen, N. Upadhyaya, and V. Vitelli, Proc. Natl. Acad. Sci. U.S.A. **111**, 13004 (2014).

[21] J. Paulose, A. S. Meussen, and V. Vitelli, Proc. Natl. Acad. Sci. U.S.A. **112**, 7639 (2015).

[22] E. Prodan and C. Prodan, Phys. Rev. Lett. **103**, 248101 (2009).

[23] H. C. Po, Y. Bahri, and A. Vishwanath, arXiv:1410.1320.

[24] M. Xiao, G. Ma, Z. Yang, P. Sheng, Z. Q. Zhang, and C. T. Chan, Nat. Phys. **11**, 240 (2015).

[25] Z. Yang, F. Gao, X. Shi, X. Lin, Z. Gao, Y. Chong, and B. Zhang, Phys. Rev. Lett. **114**, 114301 (2015).

[26] L. M. Nash, D. Kleckner, V. Vitelli, A. M. Turner, and W. T. M. Irvine, Proc. Natl. Acad. Sci. U.S.A. **112**, 14495 (2015).

[27] P. Wang, L. Lu, and K. Bertoldi, Phys. Rev. Lett. **115**, 104302 (2015).

[28] Y.-T. Wang, P.-G. Luan, and S. Zhang, New J. Phys. **17**, 073031 (2015).

[29] R. Susstrunk and S. D. Huber, Science **349**, 47 (2015).

[30] W. P. Su, J. R. Schrieffer, and A. J. Heeger, Phys. Rev. Lett. **42**, 1698 (1979).

[31] T. Hull, *Project Origami: Activities for Exploring Mathematics* (CRC Press, Boca Raton, 2012).

[32] See Supplemental Material at http://link.aps.org/supplemental/10.1103/PhysRevLett.116.135501 for additional technical details and derivations.

[33] S. Pellegrino, *Deployable Structures* (Springer-Verlag, Wien, 2001).

[34] L. Asimow and B. Roth, Trans. Am. Math. Soc. **245**, 279 (1978).

[35] C. Calladine, Int. J. Solids Struct. **14**, 161 (1978).

[36] For structures with $\kappa = 1$, that lie on the transition between the two distinct topological phases, the winding number and, hence, polarization is not defined.

[37] V. Vitelli, B. G. Chen, and N. Upadhyaya, arXiv:1407.2890.

[38] Note that by rotating the structure by 180° one ends up with a "new" unit cell with $\gamma \to -\gamma$ and $\beta \to -\beta$, which is in the opposite topological phase.

[39] More precisely, since the function $\det \mathbf{R}(\mathbf{q})$ is gauge dependent, the claim is that this is true in the gauge arising from a "balanced" unit cell as defined in Refs. [17,18].

[40] D. Z. Rocklin, B. G. Chen, M. Falk, V. Vitelli, and T. Lubensky, arXiv:1510.04970.

[41] J. Paulose, B. G. Chen, and V. Vitelli, Nat. Phys. **11**, 153 (2015).